arXiv:1611.10195v1 [cs.CV] 30 Nov 2016

# POSEidon: Face-from-Depth for Driver Pose Estimation

Guido Borghi Marco Venturelli Roberto Vezzani Rita Cucchiara
University of Modena and Reggio Emilia
name.surname@unimore.it

## Abstract

*Fast and accurate upper-body and head pose estimation is a key task for automatic monitoring of driver attention, a challenging context characterized by severe illumination changes, occlusions and extreme poses. In this work, we present a new deep learning framework for head localization and pose estimation on depth images. The core of the proposal is a regression neural network, called POSEidon, which is composed of three independent convolutional nets followed by a fusion layer, specially conceived for understanding the pose by depth. In addition, to recover the intrinsic value of face appearance for understanding head position and orientation, we propose a new Face-from-Depth approach for learning image faces from depth. Results in face reconstruction are qualitatively impressive. We test the proposed framework on two public datasets, namely Biwi Kinect Head Pose and ICT-3DHP, and on Pandora, a new challenging dataset mainly inspired by the automotive setup. Results show that our method overcomes all recent state-of-art works, running in real time at more than 30 frames per second.*

## 1. Introduction

Nowadays, we are witnessing a revolution in the automotive field, where ICT technologies are becoming sometimes more important than the engine itself. New solutions are required to solve many human-centered problems: semi-autonomous driving, driver behavior understanding, human-machine-interaction for entertainment, driver attention analysis for safe driving are just some examples. All of them, lay on the basic task of estimating the driver pose, and in particular of the face and upper body parts, which are the mainly visible items of a driver. Computer Vision research [32, 44, 4, 13, 11] achieved encouraging results, even if they are still not completely satisfactory due to some strong constraints of the context: reliability with strong pose changes, robustness to large occlusions (*e.g.* glasses), in conjunction with non-intrusive capabilities, real time and low cost requirements (Fig. 1). In addition, standard techniques based on intensity images are not always applicable, due to the poor illumination conditions during the night and the continuous illumination changes during the day. For this reasons, computer vision solutions based on illumination-insensitive data sources such as thermal [45] or depth [30] cameras are emerging.

Figure 1. Some real situations in which head and upper-body pose estimation could be useful to monitor the driver's attention level.

Therefore, we propose a complete framework for driver monitoring based on depth images only, that can be easily acquired by commercial low-cost sensors placed inside the vehicles. Starting from head localization, the ultimate goal of the framework is the estimation of the head and shoulder pose, measured as pitch, roll and yaw rotation angles. To this aim, a new triple regressive Convolutional Neural Network architecture, called *POSEidon*, is proposed, that combines depth, motion features and appearance.

One of the most innovative contribution is a *Face-from-Depth* network, that is able to reconstruct gray-level faces directly from head depth images. This solution derives from the awareness that intensity images of faces are very useful to detect head pose [1, 14]: without having intensity data we would like to have similar benefits. Gray-level faces extracted by depth images have a qualitatively impressive similarity (Fig. 2). Summarizing, the novel contributions of the paper are the following:

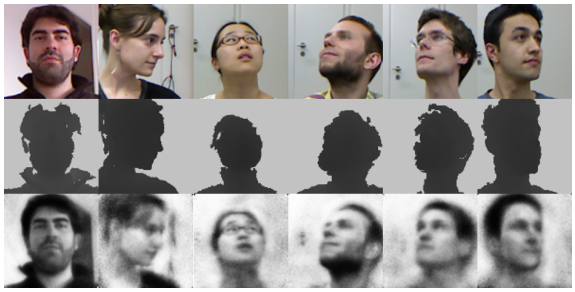

Figure 2. Examples of gray-level face images (bottom) reconstructed from the depth maps (middle). The corresponding ground truth is also shown (top). The first four subjects have been included in the training set, while the last two are completely new.

1. A complete and accurate framework, from head localization to head and shoulder pose estimation, based only on depth data, working in real time (30 fps);

2. A new *Faces-from-Depth* architecture, to reconstruct gray-level face images directly from depth maps. To the best of our knowledge, this is the first proposal of this kind of approach;

3. A new dataset, called *Pandora*, the first containing high resolution depth data with head and shoulder pose annotations.

## 2. Related Work

Head pose estimation approaches can rely on different input types: RGB images, depth maps, or both. In order to discuss related work, we adopt the classification proposed in [30, 16], updated and summarized in three main categories, namely *feature-based*, *appearance-based* and *3D model registration* approaches.

*Feature-based* methods need facial (*e.g.* nose, eyes) or pose-dependent features, that should be visible in all poses; these methods fail when features are not detected. In [27] an accurate nose localization is used for head tracking and pose estimation on depth data. Breitenstein *et al.* [7] used geometric features to identify nose candidates to produce the final pose estimation. HOG features were extracted from RGB and depth images in [49, 38], then a Multi Layer Perceptron and a linear SVM were used for feature classification. Also [47, 50, 29] needed well visible facial features on RGB input images, and [42] on 3D data. *Appearance-based* methods rely on one or more classifiers that use raw input images, trained to perform head pose estimation. In [40] RGB and depth data were combined, exploiting a neural network to perform head pose prediction. Fanelli *et al.* [16, 17, 15] trained Random Regression Forest for both head detection and pose estimation on depth images. Tulyakov *et al.* [46] used cascade tree classifiers to tackle extreme head pose estimation task. A Convolutional Neural Network based on RGB input images is exploited in [1]. Recently, in [31] a multimodal CNN was proposed to estimate gaze direction: a regression approach was only approximated through a 360-classes classifier. Synthetic RGB datasets were used to train CNNs, that generally require a huge amount of data, *e.g.* [25].

*3D model registration* approaches create a head model from the acquired data; frequently, a manual initialization is required. In [35] facial point clouds were matched with pose candidates, through a triangular surface patch descriptor. In [2] intensity and depth data were used to build a 3D constrained local method for robust facial feature tracking. In [20] a 3D morphable model is fitted, using both RGB and depth data to predict head pose. Also [2, 8, 5, 9, 6, 37] built 3D facial model for head tracking, animation and pose estimation.

Remaining methods regard head pose estimation task as an *optimization* problem: [33] used the Particle Swarm Optimization (PSO); [22], [3] exploited the Iterative Closest Point algorithm (ICP) [26]; [30] combined PSO and ICP techniques. [23] used a least-square technique to minimize the difference between the input depth change rate and the prediction rate. Besides, several works use linear or nonlinear regression with extremely low resolution images [10]. HOG features and a Gaussian locally-linear mapping model were used in [14]. Finally, recent works produce head pose estimations performing face alignment task [52].

Several works based on head pose estimation do not take in consideration head localization task. To propose a complete head pose estimation framework, it is necessary to perform a head detection, finding the complete head or a particular point, for example the head center. With RGB images Viola and Jones [48] face detector is often exploited, *e.g.* in [20, 8, 37, 2, 40]. A different approach demands the head location to a classifier, *e.g.* [16, 46]. As reported in [30], these approaches suffer due to the lack of generalization capabilities with different acquisition devices.

Only few works in literature tackle the problem of driver body pose estimation focusing only on upper-body part or in automotive context. Ito *et al.* [21] adopting an intrusive approach, placed six marker points on driver body to predict some typical driving operations. A 2D driver body tracking system was proposed in [12], but a manual initialization of the tracking model is strictly required. In [45] a thermal long-wavelength infrared video camera was used to analyze occupant position and posture. In [43] an approach for upper body tracking system using 3D head and hands movement was developed.

## 3. The POSEidon framework

An overview of the *POSEidon* framework is depicted in Figure 3. The final goal is the estimation of the pose of the driver's head and shoulders, defined as the mass

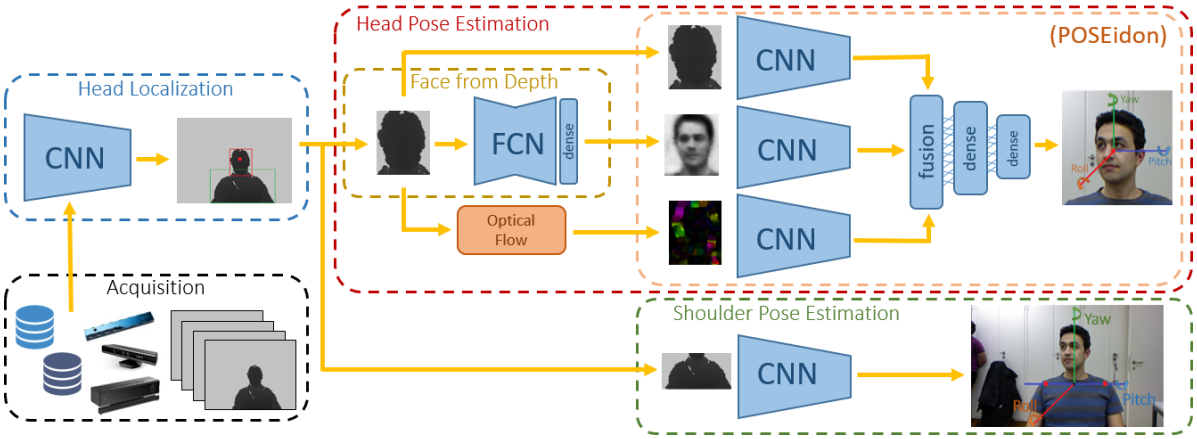


Figure 3. Overview of the whole *POSEidon* framework. Depth input images are acquired by low cost sensors (black) and provided to a Head Localization CNN (blue) to suitably crop the images around the upper-body or head regions. The first is exploited by the shoulder pose estimation task (green), while the second is selected for the head pose estimation (red) obtained through the *POSEidon* network (orange). In the center, the *Face-from-Depth* net (yellow) which produces gray-level images of the face from the depth map. [best in color]

center position and the corresponding orientation relatively to the reference frame of the acquisition device [32]. The orientation is represented using the three *pitch*, *roll* and *yaw* rotation angles. *POSEidon* directly processes the stream of depth frames captured in real time by a commercial sensor (*e.g.*, Microsoft Kinect). Position and size of the head in the foreground are estimated by a head localization module based on a regressive CNN (Sect. 5.1). The output provided is used to crop the input frames around the head or the shoulder bounding boxes, depending on the further pipeline type. Frames cropped around the head are fed to the head pose estimation block, while the others are exploited to estimate the shoulders pose. The core components of the system are the *Face-from-Depth* network (Sect. 4), and *POSEidon* (Sect. 5.2), the network which gives the name to the whole framework. Its trident shape is due to the three included CNNs, each working on likewise sources: depth, *Face-from-Depth* and motion data. The first one – *i.e.*, the CNN directly working on depth data – plays the main role on the pose estimation, while the other two cooperate to reduce the estimation error.

## 4. Face-from-Depth network

*Face-from-Depth* is one of the most innovative elements of the framework. Due to illumination issues, the appearance of the face is not always available in many scenarios, *e.g.* inside a vehicle. On the contrary, depth maps are invariant to illumination conditions but lacks of useful texture details. We aim at investigating if it is possible to imagine the appearance of a face given the corresponding depth data. Somehow, we are trying to emulate the behavior of a blind person when he tries to figure out the appearance of a friend through the touch.

The *Face-from-Depth* network has been created to this goal, even if the output is not always realistic and visually pleasant. However, the promising results confirm their positive contribution in the estimation of the head pose.

The proposed architecture fuses the key aspects of autoencoders and fully convolutional deep networks: seven convolutional layers act as a coding phase and are followed by seven symmetrical layers performing a decoding phase (Fig. 4). A single $2 \times 2$ max pooling layer has been inserted after the second layer, and a corresponding up-sampling layer after the thirteenth. Besides, two zero padding layers are added after the first and the second convolutional layers, respectively. The last layer of the network is fully connected and is exploited to have an output image with the same size of the input. We train the network with input head images resized to $64 \times 64$ pixels and with a minibatch of 32 images. The hyperbolic tangent activation function is used and best training performances are reached through the self adaptive Adadelta optimizer [51]. A specific loss function is exploited to highlight the central area of the head:

$$L = \frac{1}{R \cdot C} \sum_{i}^{R} \sum_{j}^{C} \left( ||y_{ij} - \bar{y}_{ij}||_2^2 \cdot w_{ij}^{\mathcal{N}} \right) \qquad (1)$$

where $R, C$ are the number of rows and columns of the input images, respectively. $y_{ij}, \bar{y}_{ij} \in \mathcal{R}^{ch}$ are the intensity values from the ground truth and the predicted appearance images. We used single channel ($ch = 1$) gray-level images as appearance. Finally, the term $w_{ij}^{\mathcal{N}}$ introduces a bivariate Gaussian prior mask. Best results have been obtained using $\mu = [\frac{R}{2}, \frac{C}{2}]^T$ and $\Sigma = \mathbb{I} \cdot [(R/\alpha)^2, (C/\beta)^2]^T$ with $\alpha$ and $\beta$ empirically set to $3.5, 2.5$ for squared images of $R = C = 64$. Some visual examples of input, output and ground-truth images are reported in Figure 2.

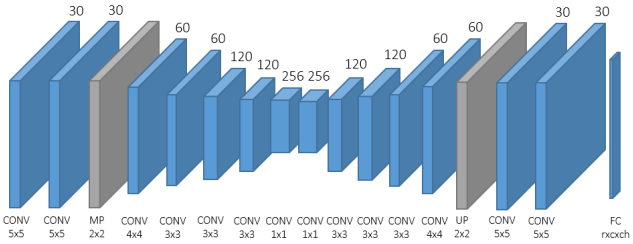
30 30 60 60 120 120 256 256 120 120 60 60 30 30
CONV 5x5 CONV 5x5 MP 2x2 CONV 4x4 CONV 3x3 CONV 3x3 CONV 3x3 CONV 1x1 CONV 1x1 CONV 3x3 CONV 3x3 CONV 3x3 CONV 4x4 UP 2x2 CONV 5x5 CONV 5x5 FC rxcxch

Figure 4. Architecture of the *Face-from-Depth* network.

# 5. Pose Estimation from depth

## 5.1. Head Localization Network

In this step we design a network to perform head localization, relying on the main assumption that a single person is in the foreground. The desired network outputs are the image coordinates $(x_H, y_H)$ of the head center, or rather, the average position of all head points in the frame [41]. Details on the deep architecture adopted are reported in Figure 5. A limited depth and small sized filters have been chosen to meet real time constraint while keeping satisfactory performance. For the same reason, input images are firstly resized to $160\times132$ pixels. 2D max pooling is run after each of the first four convolutional layers, while a dropout regularization ($\sigma = 0.5$) is exploited in fully connected layers. The hyperbolic tangent activation function is adopted, in order to map continuous output values to a predefined range $[-\infty, +\infty] \rightarrow [-1, +1]$. The network has been trained by Stochastic Gradient Descent (SGD) [24], with minibatch of size 32 and the $L_2$ loss function.
Given the head position $(x_H, y_H)$ in the frame, a dynamic size algorithm provides the head bounding box with barycenter $(x_H, y_H)$ and width $w_H$ and height $h_H$, around which the frames are cropped:

$$w_H = \frac{f_x \cdot R_x}{D}, \quad h_H = \frac{f_y \cdot R_y}{D} \tag{2}$$

where $f_x, f_y$ are the horizontal and the vertical focal lengths in pixels of the acquisition device, respectively. $R_x, R_y$ are the average width and height of a face (for head pose task $R_x = R_y = 320$) and $D$ is the distance between the head center and the acquisition device, computed averaging the depth values around the head center.
Some examples of the bounding boxes estimated by the network are superimposed in Figure 10.

## 5.2. POSEidon

The *POSEidon* network is mainly obtained as a fusion of three CNNs and has been developed to perform a regression on the 3D pose angles. As a result, continuous Euler values – corresponding to the yaw, pitch and roll angles – are estimated (see the right part of Fig. 3). The three *POSEidon* components have the same shallow architecture (see Fig. 6), but are fed with different input data types. The first network directly takes as input the head-cropped depth images; the second one is connected to the *Face-from-Depth* output and the last one operates on motion images, obtained applying the standard *Farneback* algorithm [18] on pairs of consecutive depth frames. A fusion step combines the contributions of the three above described networks: in this case, the last fully connected layer of each component is removed. Different fusion approaches that have been proposed in the past [36] are investigated. Given two feature maps $x^a, x^b$ with a certain width $w$ and height $h$, for every feature channel $d_a^x, d_b^x$ and $y \in R^{w\times h\times d}$:

- **Multiplication**: computes the element-wise product of two feature maps, as $y^{mul} = x^a \circ x^b, d^y = d_a^x = d_b^x$
- **Concatenation**: stacks two features maps, without any blend $y^{cat} = [x^a|x^b], d^y = d_a^x + d_b^x$
- **Convolution**: stacks and convolves feature maps with a filter $k$ of size $1\times1\times(d_a^x+d_b^x)/2$ and $\beta$ as bias term, $y^{conv} = y^{cat} * k + \beta, \quad d^y = (d_a^x + d_b^x)/2$

Final *POSEidon* framework exploits a combination of two fusing methods, in particular a convolution followed by a concatenation. After the fusion step, three fully connected layers composed of 128, 84 and 3 activations respectively and two dropout regularization ($\sigma = 0.5$) complete the architecture. *POSEidon* is trained with a double-step procedure. First, each composing network is trained with the following $L_2^w$ weighted loss:

$$L_2^w = \sum_{i=1}^{3} \left\| w_i \cdot (y_i - f(x_i)) \right\|_2 \tag{3}$$

where $w_i \in [0.2, 0.35, 0.45]$. This weight distribution gives more importance to the yaw angle, which is preponderant in the selected automotive context. During the individual training step, the last fully connected layer of each network is preserved. Finally, holding the weights learned for the trident components, a new training phase is carried out on

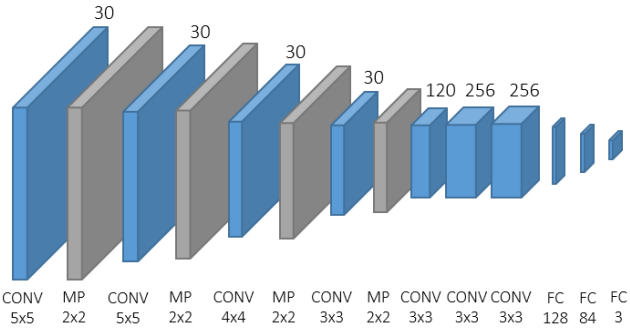


Figure 5. Architecture of the head localization network.

the last three fully connected layers of *POSEidon*, with the loss function reported in Equation 3 and minibatches of 128 images. In all training steps, the SGD optimizer [24] is exploited, the learning rate is set initially to $10^{-1}$ and then is reduced by a factor 2 every 15 epochs.

### 5.3. Shoulder pose estimation network

The framework is completed with an additional network for the estimation of the shoulders' pose. We employ the same architecture adopted for the head (see Fig. 6), performing regression on the same three pose angles. Starting from the head center position (Section 5.1), the depth input images are crop around the driver neck, using a bounding box $\{x_S, y_S, w_S, h_S\}$ with barycenter $(x_S = x_H, y_S = y_H - (h_H/4))$, and width and height obtained as described in Equation 2, but with different values of $R_x, R_y$ to produce a rectangular crop: these values are tested and discussed in Section 7. The network is trained with SGD optimizer [24], using the weighted $L_2^w$ loss function described above (see Eq. 3). Hyperbolic tangent is exploited as activation functions as usual.

## 6. Datasets

Network training and testing phases have been done exploiting two publicly available datasets, namely *Biwi Kinect Head Pose* and *ICT-3DHP*. In addition, we created a new dataset, called *Pandora*, which also contains shoulder pose annotation. Data augmentation techniques are employed to enlarge the training set, in order to achieve space invariance and avoid over fitting [24]. Random translations on vertical, horizontal and diagonal directions, jittering, zoom-in and zoom-out transformation of the original images have been exploited. Percentile-based contrast stretching, normalization and scaling of the input images are also applied to produce zero mean and unit variance data.
Follows a detailed description of the three adopted datasets.

### 6.1. Biwi Kinect Head Pose dataset

Fanelli et al. [16] introduced this dataset in 2013. It is acquired with the Microsoft Kinect sensor (structured IR light). It contains about 15k frame, with RGB ($640 \times 480$) and depth maps ($640 \times 480$). Twenty subjects have been involved in the recordings: four of them were recorded twice, for a total of 24 sequences. The ground truth of yaw, pitch and roll angles is reported together with the head center and the calibration matrix. The original paper does not report the adopted split between training and testing sets; fair comparisons are thus not guarantee. To avoid this, we clearly report the adopted split in the following.

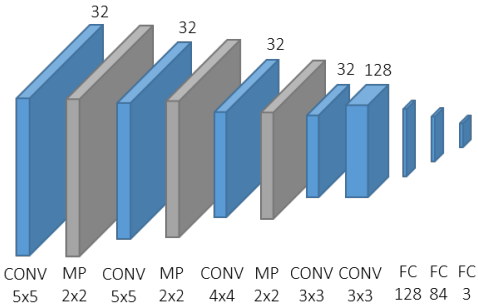


Figure 6. Architecture of the Pose Estimation networks.

Figure 7. Sample frames from the *Pandora* dataset.

### 6.2. ICT-3DHP dataset

ICT-3DHP dataset has been introduces by Baltrusaitis *et al.* in 2012 [2]. It is collected using the Microsoft Kinect sensor and contains RGB images and depth maps of about 14k frames, divided in 10 sequences. The image resolution is $640 \times 480$ pixels. An hardware sensor (*Polhemus Fastrack*) is exploited to generate the ground truth annotation. The device is placed on a white cap worn by each subject, visible in both RGB and depth frames. Moreover, the presence of few subjects and the limited number of frames make this dataset unsuitable for deep learning approaches.

### 6.3. Pandora dataset

We collect a new challenging dataset, called *Pandora*. The dataset has been specifically created for the tasks described in the paper (*i.e.*, head center localization, head pose and shoulder pose estimation) and is inspired by the automotive context. A frontal fixed device acquires the upper body part of the subjects, simulating the point of view of camera placed inside the dashboard. Among the others, the subjects also perform driving-like actions, such as grasping the steering wheel, looking to the rear-view or lateral mirrors, shifting gears and so on. *Pandora* contains 110 annotated sequences using 10 male and 12 female actors. Each subject has been recorded five times.

*Pandora* is the first publicly available dataset which combines the following features:

- **Shoulder angles**: in addition to the head pose annotation, *Pandora* contains the ground truth data of the shoulder pose expressed as yaw, pitch and roll.
- **Wide angle ranges**: subjects perform wide head ($\pm 70°$ roll, $\pm 100°$ pitch and $\pm 125°$ yaw) and shoulder ($\pm 70°$ roll, $\pm 60°$ pitch and $\pm 60°$ yaw) movements.

HEAD POSE ESTIMATION ERROR [DEG]

| Method | Year | Data | Pitch | Roll | Yaw | Avg |
|---|---|---|---|---|---|---|
| Fanelli [16] | 2011 | Depth | $8.5 \pm 9.9$ | $7.9 \pm 8.3$ | $8.9 \pm 13.0$ | $8.43 \pm 10.4$ |
| Yang [49] | 2012 | RGB + Depth | $9.1 \pm 7.4$ | $7.4 \pm 4.9$ | $8.9 \pm 8.3$ | $8.5 \pm 6.9$ |
| Padeleris [33] | 2012 | Depth | 6.6 | 6.7 | 11.1 | 8.1 |
| Rekik [37] | 2013 | RGB + Depth | 4.3 | 5.2 | 5.1 | 4.9 |
| Baltrusaitis [2] | 2012 | RGB + Depth | 5.1 | 11.3 | 6.3 | 7.6 |
| Ahn [1]* | 2014 | RGB | $3.4 \pm 2.9$ | $2.6 \pm 2.5$ | $2.8 \pm 2.4$ | $2.9 \pm 2.6$ |
| Martin [28]* | 2014 | Depth | 2.5 | 2.6 | 3.6 | 2.9 |
| Saeed [38] | 2015 | RGB + Depth | $5.0 \pm 5.8$ | $4.3 \pm 4.6$ | $3.9 \pm 4.2$ | $4.4 \pm 4.9$ |
| Papazov [35] | 2015 | Depth | $2.5 \pm 7.4$ | $3.8 \pm 16.0$ | $3.0 \pm 9.6$ | $4.0 \pm 11.0$ |
| Drouard [14] | 2015 | RGB | $5.9 \pm 4.8$ | $4.7 \pm 4.6$ | $4.9 \pm 4.1$ | $5.2 \pm 4.5$ |
| Meyer [30] | 2015 | Depth | 2.4 | 2.1 | 2.1 | 2.2 |
| Liu [25] | 2016 | RGB | $6.0 \pm 5.8$ | $5.7 \pm 7.3$ | $6.1 \pm 5.2$ | $5.9 \pm 6.1$ |
| **POSEidon** | 2016 | Depth | $\mathbf{1.6 \pm 1.7}$ | $\mathbf{1.8 \pm 1.8}$ | $\mathbf{1.7 \pm 1.5}$ | $\mathbf{1.7 \pm 1.7}$ |

Table 1. Results on *Biwi* dataset. Input cropping is done using the ground truth head position.

For each subject, two sequences are performed with constrained movements, changing the yaw, pitch and roll angles separately, while three additional sequences are completely unconstrained.

- **Challenging camouflage**: garments as well as various objects are worn or used by the subjects to create head and/or shoulder occlusions. For example, people wear prescription glasses, sun glasses, scarves, caps, and manipulate smartphones, tablets or plastic bottles.
- **Deep-learning oriented**: the dataset contains more than 250k full resolution RGB ($1920 \times 1080$ pixels) and depth images ($512 \times 424$ pixels) with the corresponding annotation.
- **Time-of-Flight (ToF) data**: a Microsoft Kinect One device is used to acquire depth data, with a better quality than other datasets created with the first Kinect version [39].

Each frame of the dataset is composed of the RGB appearance image, the corresponding depth map, the 3D coordinates of the skeleton joints corresponding to the upper body part, including the head center and the shoulders positions. For convenience's sake, the 2D coordinates of the joints on both color and depth frames are provided as well as the head and shoulder pose angles with respect to the camera reference frame. Shoulder angles are obtained through the conversion to Euler angles of a corresponding rotation matrix, obtained from a user-centered system [34] and defined by the following unit vectors $(N_1, N_2, N_3)$:

$$\begin{aligned} N_1 &= \frac{p_{RS}-p_{LS}}{\|p_{RS}-p_{LS}\|} \quad U = \frac{p_{RS}-p_{SB}}{\|p_{RS}-p_{SB}\|} \\ N_3 &= \frac{N_1 \times U}{\|N_1 \times U\|} \quad N_2 = N_1 \times N_3 \end{aligned} \tag{4}$$

where $p_{LS}$, $p_{RS}$ and $p_{SB}$ are the 3D coordinates of the left shoulder, right shoulder and spine base joints. The annotation of the head pose angles has been collected using a wearable Inertial Measurement Unit (IMU) sensor. The sensor has been worn by the subjects in a non visible position (*i.e.*, on the rear of the head) to avoid distracting artifacts on both color and depth images. The IMU sensors have been calibrated and aligned at the beginning of each sequence, assuring the reliability of the provided angles. The dataset is publicly available (`http://imagelab.ing.unimore.it/pandora/`).

(a) left (b) top (c) right (d) bottom (e) middle

Figure 8. Visual examples of the simulated occlusion types applied on a *Biwi* frame.

## 7. Experimental results

The proposed framework has been deeply tested using the datasets described in Section 6.

Each system component has been individually evaluated on *Pandora*. Sequences of subjects 10, 14, 16 and 20 have been used for testing, the remaining for training. Table 2 reports an internal evaluation, providing mean and standard deviation of the estimation errors obtained on each angle and for each system configuration. Similar to Fanelli *et al.* [16], we also report the mean accuracy as percentage of good estimations (*i.e.*, angle error below $15^\circ$). The first line of Table 2 shows the performance of a baseline system, obtained using the pose estimation network (Fig. 6) only. The captured depth frames are directly fed to the network without processing and crop. The crop step is included instead in the configurations of the other rows, using the ground truth head position as center. Results obtained using

HEAD POSE ESTIMATION ERROR [DEG]

| Architecture | Input | Cropping | Fusion | Head | | | Accuracy |
|---|---|---|---|---|---|---|---|
| | | | | Pitch | Roll | Yaw | |
| Single CNN | depth | | - | $8.1 \pm 7.1$ | $6.2 \pm 6.3$ | $11.7 \pm 12.2$ | 0.553 |
| | depth | $\surd$ | - | $6.5 \pm 6.6$ | $5.4 \pm 5.1$ | $10.4 \pm 11.8$ | 0.646 |
| | FfD | $\surd$ | - | $6.8 \pm 7.0$ | $5.7 \pm 5.7$ | $10.5 \pm 14.6$ | 0.647 |
| | gray-level | $\surd$ | - | $7.1 \pm 6.6$ | $5.6 \pm 5.8$ | $9.0 \pm 10.9$ | 0.639 |
| | MI | $\surd$ | - | $7.7 \pm 7.5$ | $5.3 \pm 5.7$ | $10.0 \pm 12.5$ | 0.609 |
| Double CNN | depth + FfD | $\surd$ | concat | $5.6 \pm 5.0$ | $4.9 \pm 5.0$ | $9.8 \pm 13.4$ | 0.698 |
| | depth + MI | $\surd$ | concat | $6.0 \pm 6.1$ | $4.5 \pm 4.8$ | $9.2 \pm 11.5$ | 0.690 |
| POSEidon | depth + FfD + MI | $\surd$ | concat | $6.3 \pm 6.1$ | $5.0 \pm 5.0$ | $10.6 \pm 14.2$ | 0.657 |
| | depth + FfD + MI | $\surd$ | mul+concat | $5.6 \pm 5.6$ | $4.9 \pm 5.2$ | $9.1 \pm 11.9$ | 0.712 |
| | depth + FfD + MI | $\surd$ | conv+concat | $5.7 \pm 5.6$ | $4.9 \pm 5.1$ | $9.0 \pm 11.9$ | 0.715 |

Table 2. Results of the head pose estimation on *Pandora* comparing different system architectures. The baseline is a single CNN working on the source depth map. The accuracy is the percentage of correct estimations ($err < 15°$). FfD: Face-from-Depth, MI: Motion Images.

single networks, couples of them and the complete *POSEidon* architecture are shown. The last row highlights the best performance reached using *conv* fusion of couples of input types, followed by the *concat* step. Even if the choice of the fusion method has a limited effect (as deeply investigated in [36, 19]), the most significant improvement of the system is reached exploiting the three input types together.

Figure 9 shows a comparison of the estimation errors made by each trident component. Each graph plots the error distribution of a specific network configuration with respect to the ground truth value. Depth data allows to reach the lowest error rates for frontal heads, while the other input data types are better in presence of rotated poses. The graphs highlight the averaging capabilities of *POSEidon* too.

Table 2 includes an indirect evaluation of the reconstruction capabilities of the *Face-from-Depth* network. The results reported on the third and forth rows are obtained using the network of Figure 6 with the reconstructed appearance image and the original gray-level images as input, respectively. The similar results confirm that the obtained image reconstruction is sufficiently accurate, at least for the pose estimation task. We compared the results of *POSEidon* with state of the art systems using the *Biwi* dataset. According with Fanelli *et al.* [16], 18 subjects are used to train the system while two for the testing. More specifically, we exploited the sequences #11 and #12 for testing and the remaining for training. Table 1 reports the corresponding results as indicated in the cited papers. *POSEidon* achieves impressive results on *Biwi* dataset: the mean error is under $2^\circ$ for all of the three angles, with a small standard deviation. The system overcomes all the reported methods, included the recent proposal by Meyer *et al.* [30]. The performance are better than the other few approaches based on deep learning, 3D data and regression [1, 31]. Moreover, *POSEidon* also overcomes the approaches working on appearance data. The proposals marked with a star (*) do not follow the same split or apply a different testing procedure. For example, authors of [1] randomly pick test samples from the dataset and do not apply a cross validation procedure. Thus, the comparison with them may not be fair. Results of [33] reported in table have been taken from [30] for the sake of comparability. As already mentioned, in real situations the driver head may be affected by severe occlusions caused by hands and objects such as smartphones, scarves, bottles and so on. Besides having included these kinds of occlusion in some *Pandora* sequences, we have carried out a specific set of experiments to test the reliability of *POSEidon* in presence of occlusions or missing data. We artificially applied the masks depicted in Figure 8 to remove parts of the input frames and simulate occlusions. The corresponding performance of *POSEidon* is shown in Table 3, which confirms the reliability of the system also in these cases. The absence of the upper body part of the head strongly impacts with the system performance, in particular for the estimation of the

| Occluded part | Head | | |
|---|---|---|---|
| | Pitch | Roll | Yaw |
| (a) left | $2.6 \pm 3.0$ | $4.0 \pm 2.9$ | $7.8 \pm 8.1$ |
| (b) top | $42.5 \pm 21.2$ | $12.3 \pm 9.3$ | $10.2 \pm 7.6$ |
| (c) right | $2.1 \pm 1.8$ | $2.8 \pm 2.6$ | $8.4 \pm 8.5$ |
| (d) bottom | $4.2 \pm 3.3$ | $4.3 \pm 3.5$ | $4.0 \pm 3.0$ |
| (e) middle | $11.0 \pm 5.3$ | $3.0 \pm 2.8$ | $6.1 \pm 4.9$ |
| random | $12.5 \pm 18.3$ | $5.3 \pm 6.1$ | $7.4 \pm 7.1$ |

Table 3. Estimation errors of POSEidon in presence of simulated occlusions. The system is fed with images from the *Biwi* dataset occluded using the masks illustrated in figure 8. Results of the last line are obtained by applying a random mask to each frame.

| Parameters | | Shoulders | | | Accuracy |
|---|---|---|---|---|---|
| $R_x$ | $R_y$ | Pitch | Roll | Yaw | |
| No crop | | $2.5 \pm 2.3$ | $3.0 \pm 2.6$ | $3.7 \pm 3.4$ | 0.877 |
| 700 | 250 | $2.9 \pm 2.6$ | $2.6 \pm 2.5$ | $4.0 \pm 4.0$ | 0.845 |
| 850 | 250 | $2.4 \pm 2.2$ | $2.5 \pm 2.2$ | $3.1 \pm 3.1$ | 0.911 |
| 850 | 500 | $\mathbf{2.2 \pm 2.1}$ | $\mathbf{2.3 \pm 2.1}$ | $\mathbf{2.9 \pm 2.9}$ | **0.924** |

Table 4. Estimation errors and mean accuracy of the shoulder pose estimation on *Pandora*

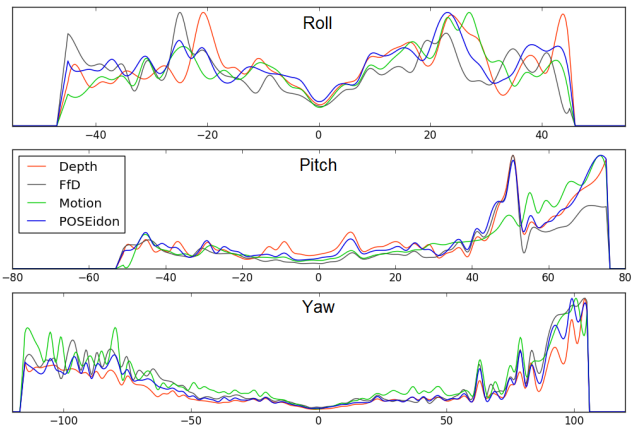


Figure 9. Error distribution of each *POSEidon* components on *Pandora* dataset. On x-axis are reported the ground truth angles, on y-axis the distribution of error for each input type.

pitch angle. Similarly, the head part around the nose plays a crucial role in the pose estimation, as highlighted by the errors generated by the occlusion type (e).

The network performing the shoulder pose estimation has been tested on *Pandora* only, due to the lack of the corresponding annotations in the other datasets. Results are reported in Table 4, where different image crops are compared. (see Section 5.3). The reported results are very promising, reaching an accuracy over 92%.

In order to have a fair comparison, results reported in Tables 1 and 2 are obtained using the ground truth head position as input to the crop procedure. We finally test the whole pipeline, including the head localization network described in section 5.1. The additional *ICT-3DHP* dataset has been adopted. The mean errors of the head localization (in pixels) and the pose estimation errors are summarized in Table 5. Sometimes, the estimated position generates a more effective crop of the head. As a result, the whole pipeline performs better on the head pose estimation over the *Biwi* dataset. *POSEidon* reaches valuable results also on the *ICT-3DHP* dataset and it provides comparable results with respect to state of the art methods working on both depth and RGB data [38, 2]. The complete framework has been implemented and tested on a desktop computer equipped with a *NVidia Quadro k2200* GPU board and on a laptop with a *NVidia GTX 860M*. Real time performance has been obtained in both cases, with a processing rate of about 30 frames per second, with a limited dedicated graphical memory requirement. Some examples of the system output are reported in Figure 10, where the six pose angles are visually shown using colored bars. In addition, the original depth map, the *Face-from-Depth* reconstruction and the motion data given in input to *POSEidon* are placed on the left of each frame. Pre-trained networks and models are publicly available.

| **Dataset** | **Loc.** | **Head** | | |
|---|---|---|---|---|
| | | Pitch | Roll | Yaw |
| Biwi | 3.27±2.19 | 1.5±1.4 | 1.7±1.7 | 2.3±2.1 |
| ICT-3DHP | - | 5.0±4.3 | 3.5±3.5 | 7.1±6.1 |
| Pandora | 4.27±3.25 | 7.6±8.5 | 4.8±4.8 | 10.6±12.7 |

Table 5. Results on *Biwi*, *ICT-3DHP* and *Pandora* dataset of the complete *POSEidon* pipeline (*i.e.*, head localization, cropping and pose estimation).

## 8. Conclusions and future work

A complete framework for head localization and pose estimation called *POSEidon* is presented. It requires no initialization and does not rely on a previous computation of specific facial features, like nose and landmarks. The system has shown impressive results also in presence of occlusions, extreme poses of head and shoulders. Besides, the use of depth data only enhances the efficacy under severe light changes and poor illumination conditions. All these aspects make the proposed framework suitable to particular challenging contexts, such as automotive. A new and high quality 3D dataset, *Pandora*, is then proposed and publicly released. *POSEidon* runs in real time on desktop and laptop computers equipped with common GPU. Thanks to the very accurate estimation of the pose of the head and shoulders, we are going to embed the *POSEidon* framework in a complete system for monitoring the driver attention level.

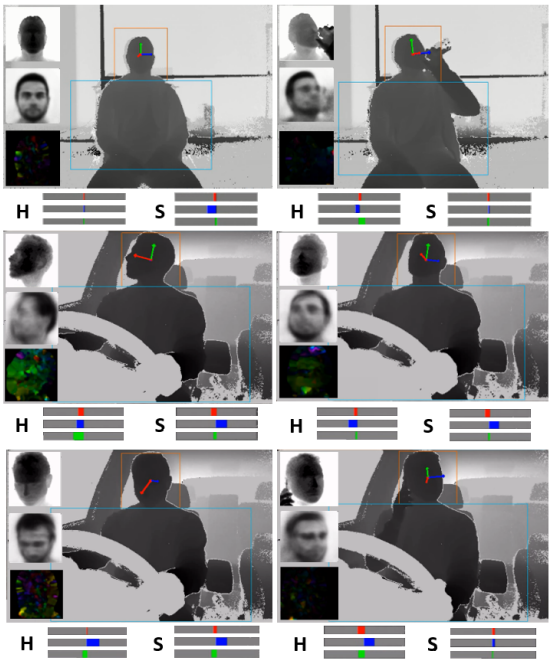


Figure 10. Visual examples of the proposed framework output. Head (H) and shoulder (S) pose angles are reported as bars centered at 0°. Depth map, *Face-from-Depth* and motion input data are depicted on the left of each frame. [best in colors]

## References


[1] B. Ahn, J. Park, and I. S. Kweon. Real-time head orientation from a monocular camera using deep neural network. pages 82–96, 2014.

[2] T. Baltrušaitis, P. Robinson, and L.-P. Morency. 3d constrained local model for rigid and non-rigid facial tracking. In *Proc. of IEEE Int. Conf. on Computer Vision and Pattern Recognition (CVPR)*, pages 2610–2617, 2012.

[3] T. Bär, J. F. Reuter, and J. M. Zöllner. Driver head pose and gaze estimation based on multi-template icp 3-d point cloud alignment. In *2012 15th International IEEE Conference on Intelligent Transportation Systems*, pages 1797–1802, 2012.

[4] L. M. Bergasa, J. Nuevo, M. A. Sotelo, R. Barea, and M. E. Lopez. Real-time system for monitoring driver vigilance. *IEEE Transactions on Intelligent Transportation Systems*, 7(1):63–77, 2006.

[5] V. Blanz and T. Vetter. A morphable model for the synthesis of 3d faces. In *Proc. of the 26th annual conference on Computer graphics and interactive techniques*, pages 187–194, 1999.

[6] A. Bleiweiss and M. Werman. Robust head pose estimation by fusing time-of-flight depth and color. In *Proc. of IEEE International Workshop on Multimedia Signal Processing (MMSP)*, pages 116–121, 2010.

[7] M. D. Breitenstein, D. Kuettel, T. Weise, L. Van Gool, and H. Pfister. Real-time face pose estimation from single range images. In *Proc. of IEEE Int. Conf. on Computer Vision and Pattern Recognition (CVPR)*, pages 1–8. IEEE, 2008.

[8] Q. Cai, D. Gallup, C. Zhang, and Z. Zhang. 3d deformable face tracking with a commodity depth camera. In *Proc. of European Conference on Computer Vision*, pages 229–242, 2010.

[9] C. Cao, Y. Weng, S. Lin, and K. Zhou. 3d shape regression for real-time facial animation. *ACM Transactions on Graphics (TOG)*, 32(4):41, 2013.

[10] J. Chen, J. Wu, K. Richter, J. Konrad, and P. Ishwar. Estimating head pose orientation using extremely low resolution images. In *2016 IEEE Southwest Symposium on Image Analysis and Interpretation (SSIAI)*, pages 65–68, 2016.

[11] B. Czupryński and A. Strupczewski. High accuracy head pose tracking survey. In *International Conference on Active Media Technology*, pages 407–420. Springer, 2014.

[12] A. Datta, Y. Sheikh, and T. Kanade. Linear motion estimation for systems of articulated planes. In *Proc. of IEEE Int. Conf. on Computer Vision and Pattern Recognition (CVPR)*, pages 1–8. IEEE, 2008.

[13] A. Doshi and M. M. Trivedi. Head and eye gaze dynamics during visual attention shifts in complex environments. *Journal of vision*, 12(2):9–9, 2012.

[14] V. Drouard, S. Ba, G. Evangelidis, A. Deleforge, and R. Horaud. Head pose estimation via probabilistic high-dimensional regression. In *Proc. of IEEE International Conference on Image Processing*, pages 4624–4628, 2015.

[15] G. Fanelli, M. Dantone, J. Gall, A. Fossati, and L. Van Gool. Random forests for real time 3d face analysis. *Int. J. Comput. Vision*, 101(3):437–458, 2013.

[16] G. Fanelli, J. Gall, and L. Van Gool. Real time head pose estimation with random regression forests. In *Proc. of IEEE Int. Conf. on Computer Vision and Pattern Recognition (CVPR)*, pages 617–624, 2011.

[17] G. Fanelli, T. Weise, J. Gall, and L. Van Gool. Real time head pose estimation from consumer depth cameras. In *Joint Pattern Recognition Symposium*, pages 101–110, 2011.

[18] G. Farneback. Very high accuracy velocity estimation using orientation tensors, parametric motion, and simultaneous segmentation of the motion field. In *Proc. of IEEE International Conference on Computer Vision*, volume 1, pages 171–177. IEEE, 2001.

[19] C. Feichtenhofer, A. Pinz, and A. Zisserman. Convolutional two-stream network fusion for video action recognition. *arXiv preprint arXiv:1604.06573*, 2016.

[20] R. S. Ghiass, O. Arandjelović, and D. Laurendeau. Highly accurate and fully automatic head pose estimation from a low quality consumer-level rgb-d sensor. In *Proc. of the 2nd Workshop on Computational Models of Social Interactions: Human-Computer-Media Communication*, pages 25–34, 2015.

[21] T. Ito and T. Kanade. Predicting driver operations inside vehicles. In *Automatic Face & Gesture Recognition, 2008. FG'08. 8th IEEE International Conference on*, pages 1–6. IEEE, 2008.

[22] J. Kennedy. Particle swarm optimization. In *Encyclopedia of machine learning*, pages 760–766. Springer, 2011.

[23] F. A. Kondori, S. Yousefi, H. Li, S. Sonning, and S. Sonning. 3d head pose estimation using the kinect. In *Proc. of International Conference on Wireless Communications and Signal Processing (WCSP)*, pages 1–4, 2011.

[24] A. Krizhevsky, I. Sutskever, and G. E. Hinton. Imagenet classification with deep convolutional neural networks. In *Advances in neural information processing systems*, pages 1097–1105, 2012.

[25] X. Liu, W. Liang, Y. Wang, S. Li, and M. Pei. 3d head pose estimation with convolutional neural network trained on synthetic images. In *Proc. of IEEE International Conference on Image Processing*, pages 1289–1293, 2016.

[26] K.-L. Low. Linear least-squares optimization for point-to-plane icp surface registration. *Techrep - Chapel Hill, University of North Carolina*, 4, 2004.

[27] S. Malassiotis and M. G. Strintzis. Robust real-time 3d head pose estimation from range data. *Pattern Recognition*, 38(8):1153–1165, 2005.

[28] M. Martin, F. v. d. Camp, and R. Stiefelhagen. Real time head model creation and head pose estimation on consumer depth cameras. In *Proceedings of the 2014 2Nd International Conference on 3D Vision - Volume 01*, 3DV '14, pages 641–648, Washington, DC, USA, 2014. IEEE Computer Society.

[29] Y. Matsumoto and A. Zelinsky. An algorithm for real-time stereo vision implementation of head pose and gaze direction measurement. In *Proc. of IEEE International Conference on Automatic Face and Gesture Recognition*, pages 499–504, 2000.

[30] G. P. Meyer, S. Gupta, I. Frosio, D. Reddy, and J. Kautz. Robust model-based 3d head pose estimation. In *Proc. of*

*IEEE International Conference on Computer Vision*, pages 3649–3657, 2015.

[31] S. S. Mukherjee and N. M. Robertson. Deep head pose: Gaze-direction estimation in multimodal video. *IEEE Transactions on Multimedia*, 17(11):2094–2107, 2015.

[32] E. Murphy-Chutorian and M. M. Trivedi. Head pose estimation in computer vision: A survey. *IEEE Trans. Pattern Anal. Mach. Intell.*, 31(4):607–626, Apr. 2009.

[33] P. Padeleris, X. Zabulis, and A. A. Argyros. Head pose estimation on depth data based on particle swarm optimization. In *Proc. of IEEE Int. Conf. on Computer Vision and Pattern Recognition Workshops (CVPRW)*, pages 42–49, 2012.

[34] G. T. Papadopoulos, A. Axenopoulos, and P. Daras. Real-time skeleton-tracking-based human action recognition using kinect data. In *International Conference on Multimedia Modeling*, pages 473–483, 2014.

[35] C. Papazov, T. K. Marks, and M. Jones. Real-time 3d head pose and facial landmark estimation from depth images using triangular surface patch features. In *Proc. of IEEE Int. Conf. on Computer Vision and Pattern Recognition (CVPR)*, pages 4722–4730, 2015.

[36] E. Park, X. Han, T. L. Berg, and A. C. Berg. Combining multiple sources of knowledge in deep cnns for action recognition. In *Proc. IEEE Winter Conference on Applications of Computer Vision (WACV)*, pages 1–8. IEEE, 2016.

[37] A. Rekik, A. Ben-Hamadou, and W. Mahdi. 3d face pose tracking using low quality depth cameras. In *VISAPP (2)*, pages 223–228, 2013.

[38] A. Saeed and A. Al-Hamadi. Boosted human head pose estimation using kinect camera. In *Proc. of IEEE International Conference on Image Processing*, pages 1752–1756, 2015.

[39] H. Sarbolandi, D. Lefloch, and A. Kolb. Kinect range sensing: Structured-light versus time-of-flight kinect. *Comput. Vis. Image Und.*, 139:1–20, 2015.

[40] E. Seemann, K. Nickel, and R. Stiefelhagen. Head pose estimation using stereo vision for human-robot interaction. In *Proc. of Sixth International Conference on Face and Gesture Recognition*, pages 626–631. IEEE Computer Society, 2004.

[41] J. Shotton, T. Sharp, A. Kipman, A. Fitzgibbon, M. Finocchio, A. Blake, M. Cook, and R. Moore. Real-time human pose recognition in parts from single depth images. *Communications of the ACM*, 56(1):116–124, 2013.

[42] Y. Sun and L. Yin. Automatic pose estimation of 3d facial models. In *Proc. of International Conference on Pattern Recognition*, pages 1–4, 2008.

[43] C. Tran and M. M. Trivedi. Introducing xmob: Extremity movement observation framework for upper body pose tracking in 3d. In *Proc. of IEEE International Symposium on Multimedia*, pages 446–447. IEEE, 2009.

[44] C. Tran and M. M. Trivedi. Vision for driver assistance: Looking at people in a vehicle. In *Visual Analysis of Humans*, pages 597–614. Springer, 2011.

[45] M. M. Trivedi, S. Y. Cheng, E. M. Childers, and S. J. Krotosky. Occupant posture analysis with stereo and thermal infrared video: Algorithms and experimental evaluation. *IEEE Transactions on Vehicular Technology*, 53(6):1698–1712, 2004.

[46] S. Tulyakov, R.-L. Vieriu, S. Semeniuta, and N. Sebe. Robust real-time extreme head pose estimation. In *Proc. of International Conference on Pattern Recognition*, pages 2263–2268, 2014.

[47] T. Vatahska, M. Bennewitz, and S. Behnke. Feature-based head pose estimation from images. pages 330–335, 2007.

[48] P. Viola and M. J. Jones. Robust real-time face detection. *Int. J. Comput. Vision*, 57(2):137–154, 2004.

[49] J. Yang, W. Liang, and Y. Jia. Face pose estimation with combined 2d and 3d hog features. In *Proc. of International Conference on Pattern Recognition*, pages 2492–2495, 2012.

[50] R. Yang and Z. Zhang. Model-based head pose tracking with stereovision. In *Proc. of IEEE International Conference on Automatic Face and Gesture Recognition*, pages 255–260, 2002.

[51] M. D. Zeiler. Adadelta: an adaptive learning rate method. *arXiv preprint arXiv:1212.5701*, 2012.

[52] X. Zhu, Z. Lei, X. Liu, H. Shi, and S. Z. Li. Face Alignment Across Large Poses: A 3D Solution. *ArXiv e-prints*, Nov. 2015.